JOURNAL OF NANO- AND ELECTRONIC PHYSICS
Vol. **18** No 1, 01007(9pp) (2026)

ЖУРНАЛ НАНО- ТА ЕЛЕКТРОННОЇ ФІЗИКИ
Том **18** № 1, 01007(9cc) (2026)

OPEN ACCESS

REGULAR ARTICLE

Effect of Synthesis Temperature on Optical Performance of ZnO-TA Nanostructures for Optoelectronic Applications

Aqilah Kamaruzaman [1,2], Nurul Akmal Che Lah[1,*] ✉

[1] *Faculty of Manufacturing and Mechatronic Engineering Technology, University Malaysia Pahang Al-Sultan Abdullah, 26600 Pekan Pahang, Malaysia*
[2] *City University Malaysia, 3500, Jalan Teknokrat 3, Cyber 4, 63000 Cyberjaya, Selangor, Malaysia*

(Received 29 December 2025; revised manuscript received 20 February 2026; published online 25 February 2026)

This study aims a comprehensive investigation into the synthesis and optical characterization of ZnO–TA nanostructures prepared via a low-temperature hydrothermal green method under controlled pH conditions. The influence of synthesis temperature was systematically examined, showing clear effects on morphology, crystallinity, and optical behavior. Structural analysis confirmed nanorods with diameters below 100 nm, while temperature variation governed aggregation and aspect ratio differences due to rapid nucleation, elevated surface energy, and incomplete crystallization. Optical and photoluminescence studies revealed that intermediate synthesis conditions produced superior transparency, favorable band gap characteristics, and balanced defect emission compared to extreme temperatures. Collectively, these results identify 70°C as the optimum synthesis temperature with nearly excellence transparency transparency, as evidenced by transmittance reaching 79% , combined with a favorable direct band gap offering ZnO–TA nanostructures with enhanced optical performance and positioning them as promising candidates for optoelectronic applications such as photodetectors and light-emitting device.

Keywords: ZnO nanostructures, Tannic acid, Optical analysis, UV Absorbance, Photoluminescence, Transmittance.

DOI: 10.21272/jnep.18(1).01007 PACS numbers: 78.67. – n, 81.07. – b

1. INTRODUCTION

Zinc Oxide (ZnO) has emerged as one of the most versatile inorganic semiconductors, capturing attention across disciplines as technology advances. The unique and tunable properties of nanostructured ZnO show excellent stability in chemically and thermally stable semiconductor materials with wide applications such as in luminescent material, supercapacitors, batteries, solar cells, photocatalysis, biosensors, biomedical and biological applications in the form of bulk crystal, thin film and pellets [1-3]. The excellent optical properties such as such as a high refractive index, strong light absorption, high quantum efficiency, and excellent luminescence efficiency drawing attention for this material as well [4-7]. The strong exciton binding energy of ZnO nanostructures allows them to be used as efficient light-emitting materials with a wide range of colors make them suitable for various optoelectronic applications [4, 8]

ZnO nanostructure have been explore with various synthesising methods including sol-gel, hydrothermal, wet-chemical and green synthesis techniques [9, 10]. The selection of the synthesising method would not only influence don the performance of the metal oxide nanostructure but also effecting on the environmental benefits. Currently, the emerging of green synthesising method have also drawing attention especially due avoidance of toxicity, cost-effective, reproducible and much more straightforward [11]. These methods were introduced to prevent the composition of unwanted or harmful by-products through the build-up of reliable, sustainable, and eco-friendly synthesis procedures by using plant extracts as capping agent [12]. In this research, Tannic Acid (TA) is the capping agent that is centrally focused due to its effective ability to form strong electrostatic interactions with the surface of the nanostructure helping to stabilize the nanostructure and increases the potential to synthesise a nanostructure with a small size distribution [13-17].

ZnO-TA nanostructures previously have been studied for their potential application in various areas due to their unique optical and electrical properties. From the finding of previous research, the bandgap of ZnO-TA narrowed to 2.92 Ev. While pure ZnO was known as a semiconductor with a bandgap of 3.37 Ev [18]. The reduction of bandgap due to the addition of TA indicates the character of the

* Correspondence e-mail: akmalcl@umpsa.edu.my

Cite this article as: A. Kamaruzaman, et al., *J. Nano- Electron. Phys.* 18 No 1, 01007 (2026) https://doi.org/10.21272/jnep.18(1).01007

nanostructures as semiconductor with higher conductivity performance. As mentioned in other research, which reconnects the relationship between bandgap value and electrical conductivity. However, while the role of TA in modifying the electronic structure has been established, other synthesis parameters such as temperature and solvent type remain less systematically investigated. These factors are known to influence nucleation dynamics, crystallinity, and defect formation, which in turn affect both the optical and electronic performance of ZnO–TA nanostructures. Thus, despite progress in understanding band gap modulation through TA incorporation, there is a clear need to examine how synthesis temperature specifically governs morphology, transparency, and photoluminescence behaviour, ultimately determining the suitability of ZnO–TA nanostructures for optoelectronic applications. However, the influence of other parameter in synthesising the ZnO-TA nanostructure such as temperature and type of solvent may also effect on the performance of the nanostructure.

The objective of this study is to investigate the influence of synthesis temperature and TA incorporation under controlled pH conditions on the morphological, chemical and optical, and characteristics of ZnO nanostructures prepared via a low-temperature hydrothermal green synthesis route. While ZnO has been extensively studied for its wide band gap and optoelectronic potential, most reports focus on conventional synthesis methods or high-temperature processes, with limited attention given to environmentally benign approaches that integrate organic additives such as TA. Furthermore, the interplay between synthesis temperature, aggregation behaviour, defect-related emissions, and transparency has not been systematically correlated to the optical performance of ZnO nanostructures. This gap highlights the need for a comprehensive analysis that bridges morphology, absorbance, transmittance, and photoluminescence, thereby establishing the optimum synthesis conditions for achieving high-quality ZnO–TA nanostructures with enhanced optical properties suitable for optoelectronic applications.

2. MATERIAL AND METHODS

2.1 Synthesising of the Nanostructure

ZnO nanostructures were synthesized via a hydrothermal technique with fixed mass of 0.5 g of zinc powder (99.9% purity, analytical grade, R&M Chemicals, Evergreen Engineering & Resources, Malaysia) was dispersed in 100 mL of distilled water under continuous stirring. Subsequently, 5 mmol (0.15 g) of trisodium citrate flakes ($Na_3C_6H_5O_7$, 99.9% purity, analytical grade, R&M Chemicals, Evergreen Engineering & Resources, Malaysia) was added as a reducing agent, resulting in a homogeneous white solution that was stirred continuously at ambient temperature. For the tannic acid-modified ZnO nanostructures (ZnO-TA), the synthesis process was continued with the addition of varying volumes of 0.1 M tannic acid (TA) to modulate the pH. A 59 mM solution of TA ($C_{76}H_{52}O_{46}$, R&M Chemicals, Evergreen Engineering & Resources, Malaysia) was prepared in 1000 mL of distilled water and subsequently added to the ZnO nanostructure solution. In the process, 60 mL of TA was added to achieve pH 5. The mixture was then transferred to a heating platform enclosed within a vacuum chamber and maintained at a minimum temperature of 50°C to enhance reaction kinetics and prevent precipitation of the compounds [19–21]. The solution was kept under stirring (800 rpm) and allowed to cool to room temperature of 27°C. The procedures are then repeated with two different synthesis temperature of 70°C and 90°C. Following synthesis, the samples were cooled to room temperature, centrifuged, and rinsed multiple times with distilled water before storage. A summary of the prepared samples is presented in Table 1.

Table 1 – Summary of hydrothermal green-synthesized ZnO–TA nanostructures prepared under varying temperature during synthesis

	Zinc Powder	Tannic Acid (TA)	Trisodium Citrate	Distilled Water	pH	Reaction Temperature
ZnO-TA/ T50	0.5 g	60 mL	5 mmol (0.15 g)	100 mL	5	50°C
ZnO-TA/ T70						70°C
ZnO-TA/ T90						90°C

2.2 Morphological Measurements

The morphological dimensions of the ZnO nanostructures and ZnO-TA nanostructures were analyzed using transmission electron microscopy (TEM, LEO Libra-120 Zeiss, Germany). Samples for TEM were prepared by depositing the suspension of the ZnO-TA nanostructure solution onto a lacey carbon-coated grid specimen holder, followed by drying under ambient conditions for 24 hours. The TEM micrographs were taken at various magnifications and subsequently analyzed with Gatan Micrograph software.

The characterization of the elemental composition and morphological structure of ZnO-TA nanostructures thin films was conducted using high-resolution imaging and compositional analysis. The surface topography was analyzed through field emission scanning electron microscopy (FESEM; Auriga, Zeiss, Germany), functioning at an accelerating voltage of 5 kV. Elemental analysis was performed using energy-dispersive X-ray spectroscopy (EDX) integrated into the LSM880-FESEM system (Carl Zeiss AG, Germany), which can achieve magnifications between ×50,000 and ×100,000. The sample were prepared with 2–3 mL of ZnO-TA nanostructure suspension was placed onto aluminium foil

and dried into a powder on a heating plate, utilising a glass layer to avoid direct thermal contact. This procedure was uniformly implemented across all samples. The dried powders were then affixed to pin stubs before being placed into the FESEM chamber for imaging and compositional analysis.

2.3 Optical Measurements

The optical characteristics of ZnO and ZnO–TA nanostructures were examined through UV–Vis absorption, transmittance and photoluminescence (PL) spectroscopy. The optical band gap was estimated from Tauc plots by plotting $h\nu$ versus $(\alpha h\nu)^2$ using the absorption coefficient, focussing on the direct band gap transition of ZnO. Photoluminescence spectra were obtained to assess emission characteristics and defect-related states. Distilled water served as the reference for both UV–Vis, transmittance and PL measurements. The testing solutions were formulated by combining 2 mL of the ZnO nanostructure solution with 5 mL of distilled water, which was then transferred into a rectangular quartz cuvette for subsequent analysis. Consistent methodologies were employed for both ZnO–TA samples to guarantee a dependable comparison.

3. RESULTS AND DISCUSSIONS

3.1 Structural and Morphological Correlation

Transmission electron microscopy (TEM imaging as shown in Fig. 3 (a) validates the successful formation of ZnO nanorod structures which demonstrate a uniform one-dimensional anisotropic growth pattern. As indicated in Fig. 1 (a), for ZnO-TA nanostructured of pH5 sample synthesised at temperature 70°C, the nanostructure evolved into elongated rods with a mean diameter of 74 ± 3.2 nm and mean length of 150 ± 15.1 nm, producing a significantly higher aspect ratio of 2.36. This indicates that TA molecules act as mild capping agents, selectively adsorbing onto nonpolar planes and facilitating anisotropic crystal growth through the controlled release of Zn^{2+} ions. The moderate acidity enhances the chelation–deprotonation equilibrium of TA, promoting the directional assembly of Zn–O coordination complexes that serve as nucleation centers for nanorod elongation [22,23]. While with different synthesizing temperature of 50°C used for synthesizing the ZnO-TA nanostructures at pH5 (Fig. 1(b)), the mean diameter slightly increases to 87 ± 2.45 nm and mean length is 150 ± 15.11 nm thus reducing the aspect ratio to 1.72. This indicates, at lower synthesis temperature, the axial growth of the nanostructure slightly reduces resulting slightly lower aspect ratios of nanorods. However, both ZnO-TA nanostructure of pH5, showing TEM micrograph, exhibiting similar morphology structure of nanorod with the the mean diameter are still below 100 nm which indicate a dimension that confers a high surface area-to-volume ratio, thereby facilitating enhanced reactivity, interfacial charge transfer, and overall material performance. This increment of average diameter attributed to the acidic conditions which significantly impact the synthesis of nanomaterials by causing the aggregation of the nanostructures and modifying the surface charge and nanoparticle stability.

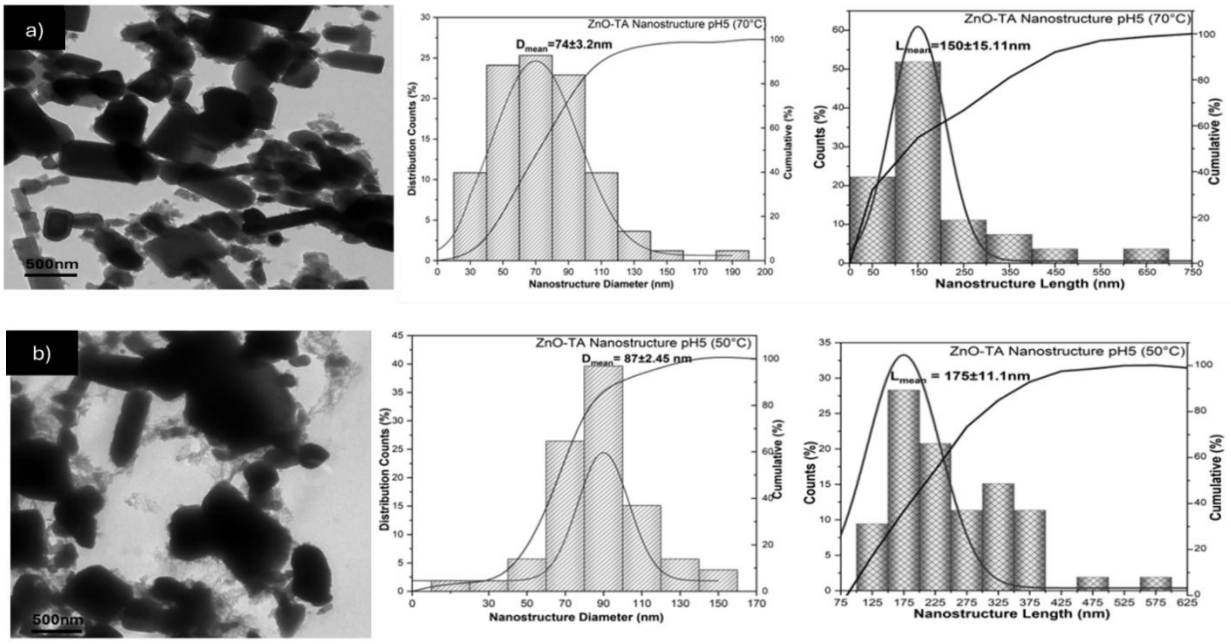

Fig. 1 – TEM images of ZnO–TA nanostructures synthesized under different pH conditions. (a) (i) ZnO–TA synthesized at Temperature of 70°C shows elongated rods with an enhanced aspect ratio, having (ii) an average diameter of 74 ± 3.2 nm and (iii) a length of 150 ± 15.1 nm. (b) (i) ZnO-TA at temperature of 50°C with similar morphology of nanorod with slightly larger (ii) an average diameter of 87 ± 2.45 nm and (iii) a length of 175 ± 11.1 nm

On supporting the surface morphology analysis, FESEM and corresponding EDX analysis was performed to examine the surface features and elemental composition of the ZnO and ZnO–TA nanostructures at 30,000× magnification. FESEM analysis further elucidates the surface morphology of the ZnO-TA nanostructures exhibit densely packed nanorod arrays as indicate in Fig. 2 (a), (b) and (c) corroborating the TEM results and confirming that moderate acidity supports directional crystal growth with enhanced structural uniformity and retain the tetrahedral nanorod morphologies. However, the introduction of TA promotes noticeable aggregation and agglomeration, particularly at synthesising temperature of 90 and 50°C. EDX analysis further indicates Zn compositions of 35.85, 68.87, and 23.76 wt.% for samples synthesized at 90°C, 70°C, and 50°C, respectively, while the corresponding O compositions are 27.57, 18.17, and 28.53 wt. %. In addition, the spectra reveal the presence of C (35.85 – 47.7 wt.%) originating from TA's phenolic groups, along with Al signals attributed to the aluminum foil substrate used during analysis. From the findings, agglomeration was more pronounced at the higher synthesis temperature of 90°C, where rapid nucleation and elevated surface energy drove particles to coalesce. Aggregation and agglomeration were also clearly visible at the lower synthesis temperature of 50°C, attributed to limited adatom mobility and incomplete crystallization that caused particles to cluster locally. In addition, significant agglomeration was observed during the drying process of the FESEM samples, as solvent evaporation induced capillary forces that promoted particle clustering in the absence of surfactants to reduce surface tension between nanostructure [24,25]. The incorporation of carbon from TA partially passivated the polar surfaces, subtly influencing rod growth while preserving tetrahedral coordination and maintaining the dominance of Zn and O composition, thereby ensuring the structural purity of the nanostructures.

3.2 Absorbance Analysis and Energy Band Gap

The optical performance through the UV–Vis absorbance spectra presented in Fig. 3 exhibit distinct changes in optical response as a function of synthesizing temperature. The optical response overall demonstrates strong absorption in the 400nm which is the range beyond blue visible region, underscoring their potential for use as active layers optoelectronic devices beyond UV application. As shown in Fig. 3, ZnO-TA nanostructure synthesis in temperature of 90°C demonstrate the absorbance at the shortest wavelength of highest wavelength of 413 nm, while as the synthesis temperature reduce to 70°C, the absorbance red shifted to 481 nm and red shifted to 428 nm as the synthesis temperature reduce to 50°C. the trend are similar as in morphological structure where synthesizing temperature of 90°C and 50°C exhibit red shifting in the absorbance spectra thus confirm the influence of aggregation as it alters the optical response by increasing Mie scattering and introducing defect-rich grain boundaries. Besides, this clustering effect also reduces exciton mobility and modifies local dielectric environments, allowing higher-energy photons to be absorbed more efficiently at shorter wavelengths. Furthermore, the red shifting attributed to several structural and morphological factors, including nanorod structure which explain greater aspect ratio and increased length of the nanorods weaken the quantum confinement effect.

This shift reflects a reduction in optical band gap energy, attributed to defect-state coupling and localized electronic interactions induced by TA coordination on ZnO surfaces. The result signifies enhanced electronic delocalization and band structure modification associated with the elongated nanorod morphology observed. Importantly, these optical characterizations provide the key insights into the electronic transition behavior and defect-mediated processes within the ZnO and TA-modified ZnO nanostructures, establishing a direct link between morphological evolution and charge transport mechanisms. The red-shifted absorption and reduced band gap correlate with its enhanced electron mobility and moderate carrier concentration, evidencing that TA-induced surface passivation not only tailors' optical transitions but also suppresses charge-trapping defects. The protonation enhances adsorption of TA onto ZnO, increasing surface coverage and amplifying these organic-associated optical features [26].

In agreement with the optical absorption trends, the variation in band gap energy elucidates on the TA incorporation, pH modulation, and morphological evolution collectively influence the electronic transitions and charge transport in ZnO nanostructures as shown in Fig 4(a) and (b), Tauc plot analysis reveals that ZnO–TA nanostructures synthesized at pH 5 exhibit slightly higher direct band gaps in the range of 3.72–3.78 eV. Specifically, the direct band gaps measured were 3.72, 3.78, and 3.74 eV for synthesis temperatures of 50, 70, and 90 °C, respectively. The slight increment observed at 70 °C is attributed to morphological shifts that enhance quantum confinement, thereby shifting both conduction and valence band edges. The difference in the direct band gap is considered significant as the value indicates a shifting of the absorption and emission wavelength which impacts the colour and efficiency of light emission and substantially affect the optical and electronic properties of the nanostructures [27,28]. From the Fig 4 (b), a slight difference is also noticed between direct and indirect band gap at 70 °C, the direct band gap measured 3.78eV while indirect band gap is 3.76eV. Smaller deviation of 0.02eV suggest the introduction of phonon assisted transitions which commonly associated with indirect band gap characteristics. However, due to very minimal difference implies that the nanostructures are influence largely by the direct band gap semiconductor characteristic. These findings collectively reveal the optical and electrical responses of the ZnO nanostructures are critically governed by the interplay between protonation-induced surface chemistry and morphology-driven quantum confinement.

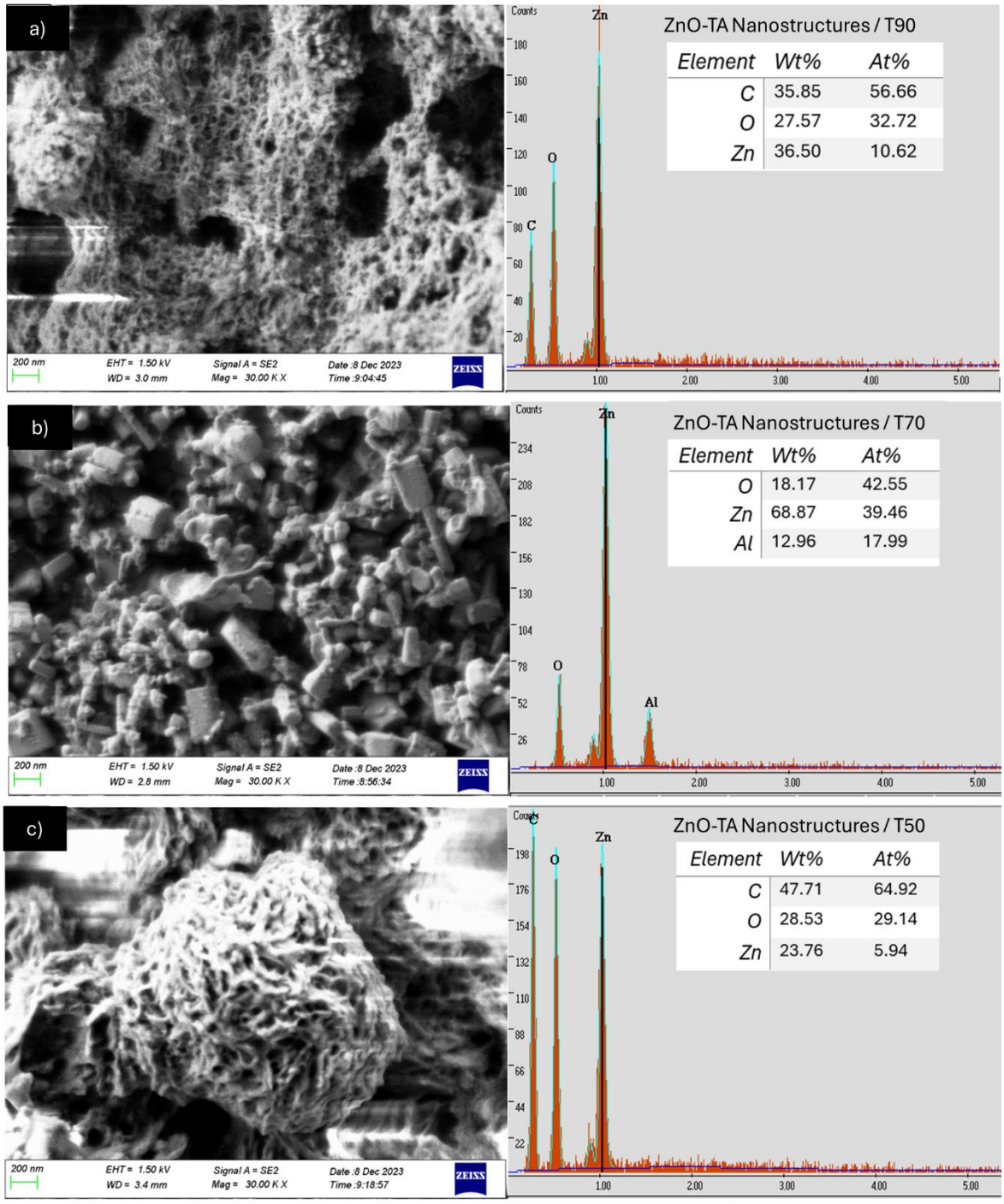

Fig. 2 – Surface morphology and elemental composition of d ZnO–TA nanostructures synthesized at varying temperature, (a)ZnO-TA nanostructures/T90, (b) ZnO-TA nanostructures/T70 and (c) ZnO-TA nanostructures/T50 display compact nanorods. EDS spectra confirm Zn and O as principal elements with trace of C from phenolic group of TA and Al arises from the FESEM substrate

3.3 Photoluminescence and Transmittance Analysis

In photoluminescence spectroscopy (PL) analysis as per shown in Fig. 5, two distinctive types of luminescent behaviour which is near band-edge (NBE) emission and deep level (DL) emission play a crucial role in describing valuable information about the nanostructure's properties [29, 30]. The less prominent peak (indicated by a yellow line) in the spectrum is associated with NBE while the prominent peak (indicated by a green line) associated with DL emission. The influenced of

temperature on the photoluminescence spectra of ZnO-TA nanostructures are monitored with samples synthesized at 50°C, 70°C, and 90°C exhibit notable differences in emission peak positions and intensities as illustrated in Fig. 5. At 50°C, the near band edge (NBE) emission peaks at 486 nm, while the deep-level (DL) emission is centred at 582 nm. For sample synthesised in 70°C, the NBE emission shifts to 474 nm with a DL peak at 572 nm. Whilst, for sample synthesised in 70°C, shows a broad emission peak of DL around 548 nm and NBE emission slightly shifting to 468nm. In the same figure, the PL emission intensities are compared across the three temperatures. Quantitatively, the NBE: DL intensity ratios were 1:14 for 50°C, 1:6 for 70°C, and 1:4 for 90°C, confirming that DL emission dominates in all cases but is progressively suppressed at higher synthesis temperatures. In lower synthesis temperature, the nanostructures exhibit the highest DL emission with NBE:DL ratio reflecting a high density of intrinsic defects, likely oxygen vacancies and interstitial zinc due to larger diameter rods increase the surface area prone to defect formation [31]. Besides the additional carbonyl group from higher atmospheric adsorption in lower temperatures which introduces additional localized states within the band gap and facilitates lower-energy radiative recombination, thereby producing the red-shifted DL emission [32].

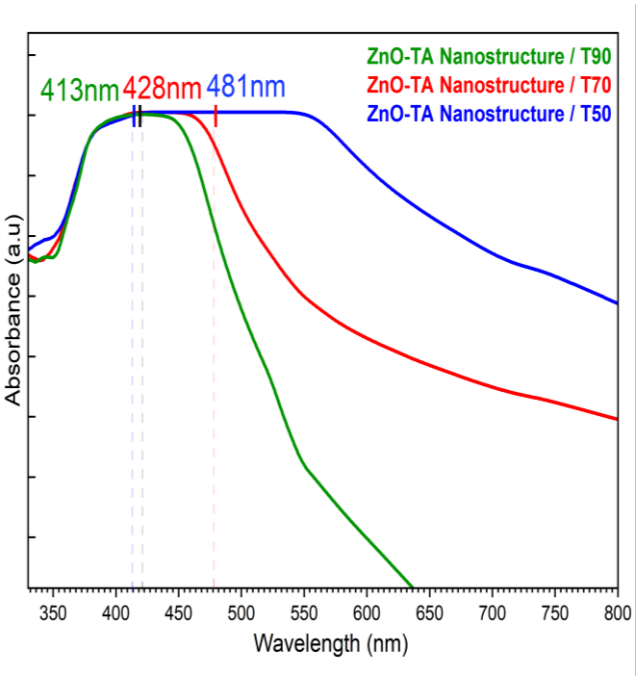

Fig. 3 – UV–Vis absorbance spectra of ZnO and ZnO–TA thin films synthesized at varying temperature of 50, 70 and 90°C. it was shown as the synthesis temperature increasing, the absorbance reflected to shorter wavelength

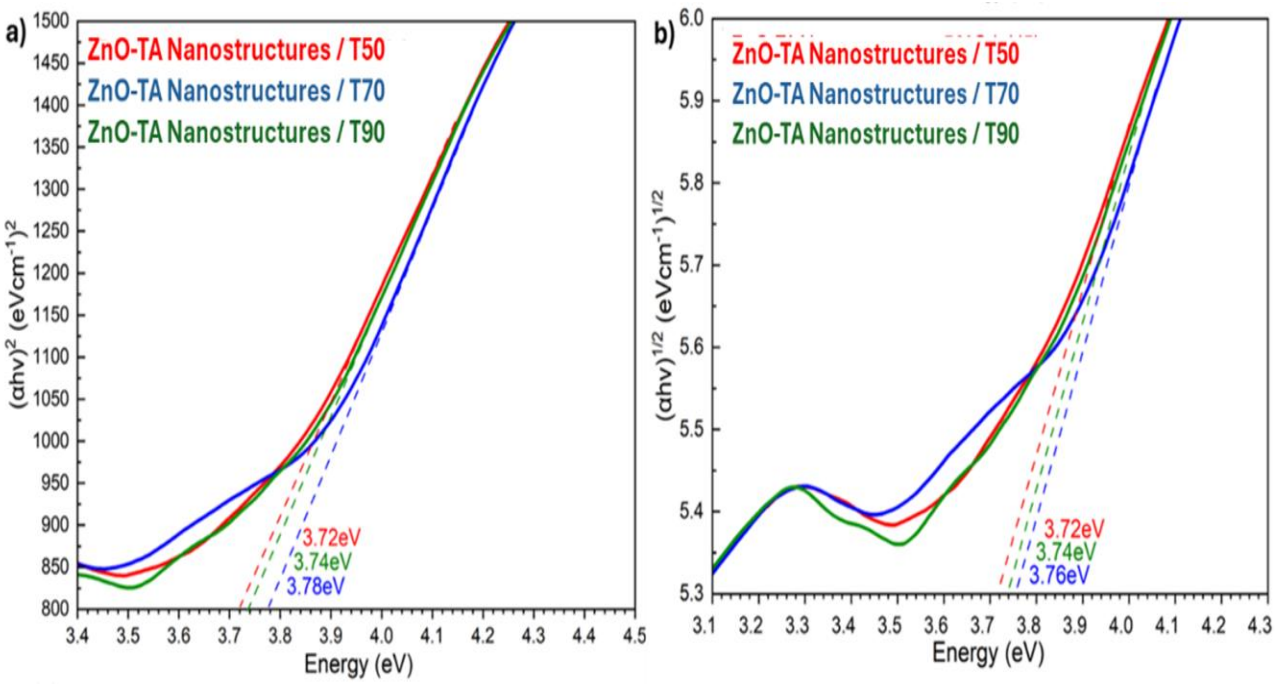

Fig. 4 – Tauc plot analysis of ZnO and TA-modified ZnO thin films synthesized at varying pH conditions, showing direct optical band gaps of 3.72 eV (ZnO–TA/T50), 3.78 eV (ZnO–TA/T70), and 3.74 eV (ZnO/T90). The slight band gap narrowing at pH5 reflects enhanced electronic coupling and defect passivation induced by TA coordination, consistent with improved charge transport behavior. The indirect band gap reflect similar values except of ZnO-TA/T70 with indirect bandgap of 3.76 eV

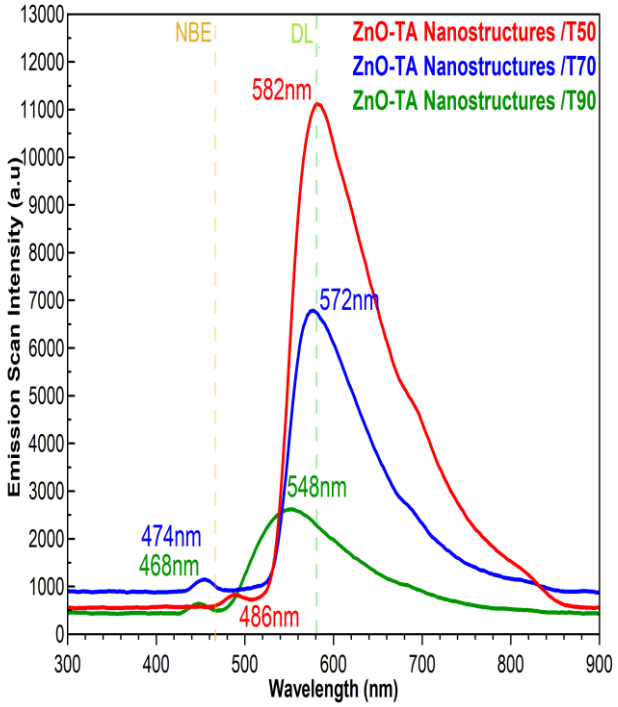

Fig. 5 – Normalized room-temperature photoluminescence (PL) emission spectra of ZnO–TA nanostructures synthesized at pH5 under different temperatures. The black peak corresponds to ZnO–TA nanostructures synthesized at 90°C, while the red and blue peaks correspond to those synthesized at 70°C and 50°C, respectively

A comparative analysis was conducted on the transmittance spectra of both ZnO and ZnO-TA nanostructures. Fig. 6 display good optical transmittance of colloidal dispersion for ZnO and ZnO-TA nanostructure within the range of 70% to 80% within wavelength of 250 nm to 600 nm with distinct absorption at the band edge 280 to 380 nm. It is important to mention that the transmittance percentage value is better compared to previously published pure ZnO nanostructure without any doping [33, 34]. For ZnO-TA nanostructure of pH5, the transmission values obtained are 75%, 79% and 71% for sample synthesis at temperatures of 50°C, 70 and 90°C, respectively. It was noticed, sample synthesis in temperature 70°C reflecting to nearly excellent transparency. This high transmittance indicates reduced scattering and uniform nanorod alignment, allowing efficient passage of visible light and highlighting the suitability of the nanostructure for optoelectronic applications requiring transparent active layers. Besides, the transmittance percentage increase significantly with the introduction of TA due to the morphological characteristic. Besides, the clear correlation was observed as ZnO-TA sample are having slightly higher bandgap due to reduces defect-related tailing, exhibit higher transmittance percentage attribute from optical transitions allowed more visible light to pass through.

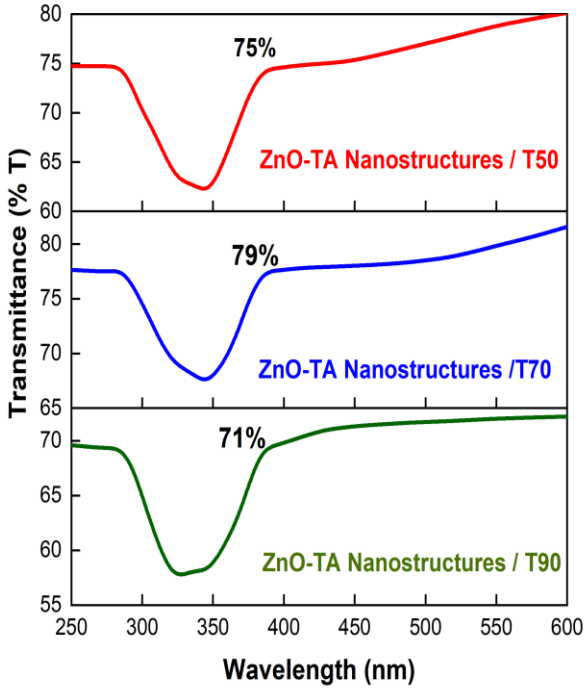

Fig. 6 – Transmittance analysis of ZnO–TA nanostructures synthesized at different temperatures, demonstrating good optical transparency across all three conditions. Notably, the sample prepared at 70°C exhibits nearly excellent transparency, reaching up to 79%.

3.4 Chemical Analysis

The FTIR analysis further consolidates the optical behaviors previously discussed, elucidating the interfacial chemistry that governs charge transport and electronic transitions within the ZnO–TA nanostructures. As shown in Fig. 7, the ZnO-TA nanostructure exhibits main stretching around 750 – 900 cm^{-1} was referred with the presence of ZnO nanostructures [35–37]. Besides, broad peak stretching was observed attribute the hydroxyl bonding due to dehydration for sample synthesis in all three temperatures was relatively within a similar range of 3200 to 3300 cm^{-1} [38, 39]. The samples synthesized at all three temperatures exhibit nearly similar peak stretching, indicating comparable compound composition; however, a noticeable difference is observed in the fingerprint region (pink shaded region), where the number of stretching vibrations increases within the range of 1070 and 1700 cm^{-1} with synthesising temperatures of 50°C and 90°C accordingly. This attribute to higher concentration of group O-C-O bonding, C=O and C-O bonding which also refers to carbonyl group characteristics which refer to higher atmospheric adsorption during the synthesising of the sample under vacuum conditions. [40–42] The lower temperature of 50°C reflects to longer time of synthesising which caused more atmospheric adsorption to occur. While a higher temperature of 90°C was nearly reaching the boiling

temperature, resulting the solvent molecule (distilled water) on having enough energy to overcome the intermolecular forces and transition from the liquid phase to the gas phase and increase of kinetic energy enhancing the collision and adsorb into surfaces of atmospheres [43].

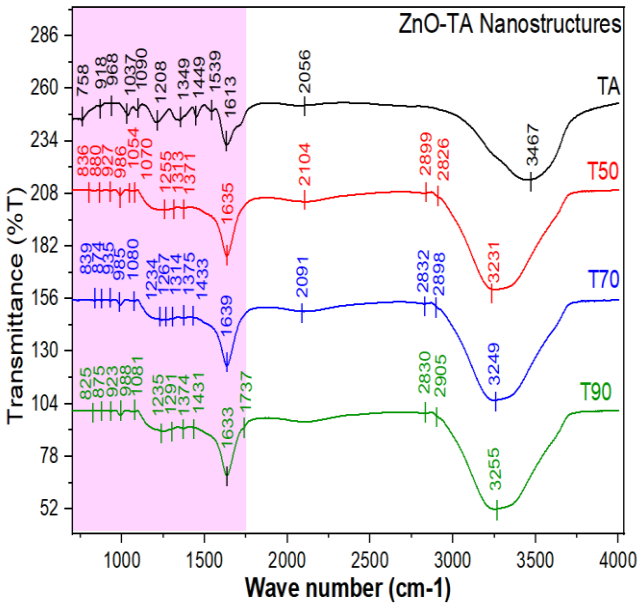

Fig. 7 – FTIR analysis of ZnO- TA nanostructures synthesis at pH 5 with different synthesising temperatures, highlighting Zn–O stretching and O–H vibrations in pristine ZnO and the emergence of aromatic C=C and carbonyl (C=O) bands

4. CONCLUSION

In summary, ZnO–TA nanostructures were successfully synthesized under controlled pH conditions and varying synthesis temperatures. The morphological analysis through FESEM and TEM revealed that TA incorporation significantly influenced nanostructure of ZnO-TA with average diameters lower than 100 nm. At higher temperature of 90°C and lower temperature of 50°C, pronounced aggregation and agglomeration were observed due to rapid nucleation with elevated surface energy and conversely, limited adatom mobility and incomplete crystallization. Besides, temperature variation also result into nanorod with different aspect ratios which also influence the overall performance of the nanostructures synthesis. Furthermore, the optical characterisation analysis revealed, ZnO-TA nanostructures synthesis in 70°C exhibited absorbance at longer wavelengths, corresponding to improved transparency as supported by transmittance analysis. Photoluminescence analysis further reinforced these findings, showing that lower synthesis temperatures produced stronger deep-level (DL) emission with a reduced NBE:DL ratio, indicative of higher defect density. This enhances visible-light emission and broadens the optical spectrum, improving suitability for applications such as photodetectors and light-emitting devices, while still retaining the direct band gap nature of ZnO. Collectively, the findings on this research deduced that 70°C represent the optimum temperature for low-temperature hydrothermal green synthesis of synthesizing ZnO-TA nanostructures with significant optical characteristics.

ACKNOWLEDGEMENTS

Authors are grateful to the Editor-in-Chief of the Journal of Nano- and Electronic Physics Protsenko Ivan Yuhymovych for a critical reading of the manuscript and his valuable comments.

The research work is entirely funded by the internal grants of Universiti Malaysia Pahang Al- Sultan Abdullah (RDU2203105).

REFERENCES

1. R. Yan, T. Takahashi, H. Zeng, T. Hosomi, M. Kanai, G. Zhang, et al, *ACS Appl. Electron. Mater.* **3**, 2925 (2021).
2. M. Laurenti, S. Stassi, G. Canavese, V. Cauda, *Adv. Mater. Interfaces* **4**, 1600758 (2017).
3. M.S. Selim, M.A. Shenashen, A. Elmarakbi, N.A. Fatthallah, S. Hasegawa, S.A. El- Safty, *Chem. Eng. J.* **320**, 653 (2017).
4. A. Wei, L. Pan, W. Huang, *Mater. Sci. Eng.: B* **176**, 1409 (2011).
5. A.D. Faisal, R.A. Ismail, W.K. Khalef, E.T. Salim, *Opt. Quantum Electron.* **52**, 212 (2020).
6. B. Anand, S.R. Krishnan, R. Podila, S. Siva Sankara Sai, A.M. Rao, R. Philip, *Phys. Chem. Chem. Phys.* **16**, 8168 (2014).
7. D.J. Gargas, H. Gao, H. Wang, P. Yang, *Nano Lett.* **11**, 3792 (2011).
8. G.C. Park, S.M. Hwang, S.M. Lee, J.H. Choi, K.M. Song, H.Y. Kim, et al, *Sci. Rep.* **5**, 10410 (2015).
9. E. Selvarajan, V. Mohanasrinivasan, *Mater. Lett.* **112**, 180 (2013).
10. O.O. Akinlotan, U.V. Ezenobi, *J. Chem. Soc. Nigeria* 45 (2020).
11. R. Kalaiarasi, N. Jayallakshmi, P. Venkatachalam, *Plant Cell Biotechnol. Mol. Biol.* **11**, 1 (2010).
12. J. Singh, T. Dutta, K.H. Kim, M. Rawat, P. Samddar, P. Kumar, *J. Nanobiotechnology* **16**, 84 (2018).
13. P. Orlowski, M. Zmigrodzka, E. Tomaszewska, K. Ranoszek-Soliwoda, M. Czupryn, M. Antos-Bielska, et al, *Int. J. Nanomedicine* **13**, 991 (2018).
14. R. la Spina, D. Mehn, F. Fumagalli, M. Holland, F. Reniero, F. Rossi, et al, *Nanomaterials* **10**, 2013 (2020).
15. M. Krzyzowska, E. Tomaszewska, K. Ranoszek-Soliwoda, K. Bien, P. Orlowski, G. Celichowski, et al, *Nanostruct. Oral Medicine*, 335 (2017).
16. J. Luo, J. Lai, N. Zhang, Y. Liu, R. Liu, X. Liu, *ACS Sustain Chem. Eng.* **4**, 1404 (2016).
17. K. Ranoszek-Soliwoda, E. Tomaszewska, E. Socha, P. Krzyczmonik, A. Ignaczak, P. Orlowski, et al, *J. Nanoparticle Research* **19**, 273 (2017).

18. T.V. Ha Luu, N.N. Dao, H.A. Le Pham, Q.B. Nguyen, V.C. Nguyen, P.H. Dang, *RSC Adv.* **13**, 5208 (2023).
19. K. Sekar, R. Nakar, J. Bouclé, R. Doineau, K. Nadaud, B. Schmaltz, et al, *Nanomaterials* **12**, 2093 (2022).
20. A. Ainun Rahmahwati, M.F. Hashim, I.L.K. Kamardin, *Adv. Mat. Res.* **1125**, 126 (2015).
21. F.T.Z. Toma, M.S. Rahman, K.H. Maria, *Discov. Mater.* **5**, 60 (2025).
22. Y. Wang, Y. Coppel, C. Lepetit, J.D. Marty, C. Mingotaud, M.L. Kahn, *Nanoscale Adv.* **3**, 6088 (2021).
23. Z. Zhao, Y. Wang, C. Delmas, C. Mingotaud, J.D. Marty, M.L. Kahn, *Nanoscale Adv.* **3**, 6696 (2021).
24. D.T. Donia, E.M. Bauer, M. Missori, L. Roselli, D. Cecchetti, P. Tagliatesta, et al, *Symmetry* (Basel) **13**, 733 (2021).
25. A.H. Abdelmohsen, W.M.A. El Rouby, N. Ismail, A.A. Farghali, *Sci. Rep.* **7**, 5946 (2017).
26. N.A. Che Lah, A. Kamaruzaman, *Sci. Rep.* **14**, 18596 (2024).
27. B.R. Borodin, I.A. Eliseyev, A.I. Galimov, L.V. Kotova, M.V. Durnev, T.V. Shubina, et al, *Phys. Rev. Mater.* **8**, 14001 (2024).
28. K. Davis, R. Yarbrough, M. Froeschle, J. White, H. Rathnayake, *RSC Adv.* **9**, 14638 (2019).
29. M.A. Reshchikov, *J. Appl. Phys.* **129**, 121101 (2021).
30. A.C. Gandhi, S.Y. Wu, *Nanomaterials* **7**, 231 (2017).
31. E.G. Barbagiovanni, V. Strano, G. Franzò, I. Crupi, S. Mirabella, *Appl. Phys. Lett.* **106**, 093108 (2015).
32. K. Nagpal, E. Rauwel, E. Estephan, M.R. Soares, P.Rauwel, *Nanomaterials* **12**, 3546 (2022).
33. A.F. Abdulrahman, S.M. Ahmed, S.M. Hamad, A.A. Barzinjy, *J. Electron. Mater.* **50**, 1482 (2021).
34. K. Lefatshe, P. Dube, D. Sebuso, M. Madhuku, C. Muiva, *Ceram. Int.* **47**, 7407 (2021).
35. S.W. Balogun, O.O. James, Y.K. Sanusi, O.H. Olayinka, *SN Appl. Sci.* **2**, 504 (2020).
36. C. Amutha, S. Thanikaikarasan, V. Ramadas, S.A. Bahadur, B. Natarajan, R. Kalyani, *Optik (Stuttg)* **127**, 4281 (2016).
37. A. Kumar, C. Khatana, D. Kumar, A. Kumari, *J. Pure Appl. Microbiol.* **15**, 1907 (2021).
38. R. Krithika, R. Balasasirekha, *J. Adv. Sci. Research* **12** (2021).
39. M. Mecozzi, E. Sturchio, *J. Imaging* **3**, 11 (2017).
40. F.B. Meng, J.J. Li, Q. Zhang, Y.C. Li, D.Y. Liu, W.J.Chen, et al., *J. Sci. Food Agric.* **101**, 4605 (2021).
41. M. Sahu, V.R.M. Reddy, B. Kim, B. Patro, C. Park, W.K. Kim, et al, *Materials* **15**, 1708 (2022).
42. G.R. Dillip, A.N. Banerjee, V.C. Anitha, S.W. Joo, B.K. Min, S.Y. Sawant, et al, *ChemPhysChem* **16**, 3214 (2015).
43. H.J. Kreuzer, Kinetics of Adsorption, *Desorption and Reactions at Surfaces In: Rocca Mario and Rahman TS and VL, editor. Springer Handbook of Surface Science*, 1035 (Cham: Springer International Publishing: 2020).

Вплив температури синтезу на оптичні характеристики наноструктур ZnO-TA для оптоелектронних застосувань

Aqilah Kamaruzaman[1,2], Nurul Akmal Che Lah[1]

[1] *Faculty of Manufacturing and Mechatronic Engineering Technology, University Malaysia Pahang Al-Sultan Abdullah, 26600 Pekan Pahang, Malaysia*
[2] *City University Malaysia, 3500, Jalan Teknokrat 3, Cyber 4, 63000 Cyberjaya, Selangor, Malaysia*

Це дослідження має на меті комплексне вивчення синтезу та оптичної характеристики наноструктур ZnO–TA, отриманих низькотемпературним гідротермальним зеленим методом за контрольованих умов pH. Вплив температури синтезу було систематично досліджено, що показало чіткий вплив на морфологію, кристалічність та оптичну поведінку. Структурний аналіз підтвердив наявність наностержнів діаметром менше 100 нм, тоді як варіація температури визначала агрегацію та відмінності у співвідношенні сторін через швидке зародження, підвищену поверхневу енергію та неповну кристалізацію. Оптичні та фотолюмінесцентні дослідження показали, що проміжні умови синтезу забезпечують кращу прозорість, сприятливі характеристики ширини забороненої зони та збалансовану емісію дефектів порівняно з екстремальними температурами. У сукупності ці результати визначають 70°C як оптимальну температуру синтезу з майже ідеальною прозорістю, про що свідчить пропускання, що досягає 79%, у поєднанні зі сприятливою шириною прямої забороненої зони, що пропонує наноструктури ZnO–TA з покращеними оптичними характеристиками та позиціонує їх як перспективних кандидатів для оптоелектронних застосувань, таких як фотодетектори та світловипромінювальні пристрої.

Ключові слова: Наноструктури ZnO, Дубильна кислота, Оптичний аналіз, УФ-поглинання, Фотолюмінесценція, Пропускання.